RSC Advances

Rapid hydrogenation: Perfect Quasi Architecture (Ag@SiO2NPs) as a substrate for Nitrophenol Reduction

Journal:	*RSC Advances*
Manuscript ID:	RA-ART-08-2014-008885.R1
Article Type:	Paper
Date Submitted by the Author:	09-Oct-2014
Complete List of Authors:	Ramalingam, Sathya; Central Leather Research Institute, Chemical Laboratory Devi, Loganathan Bhavani; Central Leather Research Institute, Chemical Lab Jonnalagadda, Raghava Rao; Central Leather Research Institute, Chemical Laboratory Unni Nair, Bala; Central Leather Research Institute, Chemical Laboratory

Rapid hydrogenation: Perfect Quasi Architecture ($Ag@SiO_2NPs$) as a substrate for Nitrophenol Reduction

Sathya Ramalingam, Loganathan Bhavani Devi, Jonnalagadda Raghava Rao*, and Balachandran Unni Nair

Chemical Laboratory, Council of Scientific & Industrial Research- Central Leather Research Institute, Adyar, Chennai-6000 20, India

*Corresponding Author: jrrao@clri.res.in; Tel. +91 44 2441 1630

Abstract

Spherical nanoparticle with Core-frame architecture is a viable route to combine multiple functionalities on a nanoscopic scale. Amongst, metal polymeric hybrid nanostructures exhibit significantly enhanced stability. Synergistic catalytic responses arise from quasi perfect morphology and their unique interactions between the metal and reactant substrate. Core-frame silver supported silica nanoparticles ($Ag@SiO_2NPs$) with different frame thickness were tailored in a controlled manner through oversimplified environmental friendly route that using simple chemical additives instead of dendrimers, linkers for prior modification of AgNPs. Here the optical and thermal studies of $Ag@SiO_2NPs$ was studied by High resolution transmission electron microscopy (HRTEM), Dynamic Light Scattering (DLS), Fourier transform infrared spectroscopy (FTIR), and Thermogravimetric analysis (TGA). The resulting stabilised nature of $Ag@SiO_2NPs$, their functionalization and environmental behaviour was analysed in detail through absorbance measurements. The control over the particle geometry provided opportunity to utilise this hybrid NPs as a temper for faster hydrogenation of p-nitrophenol with minimal reductant concentration ($NaBH_4$-3mM). Effect of volume ratio of hybrid catalyst with respect to thermal behaviour and their hydrogenation reaction time, average reaction rate, hybrid reusability were thoroughly investigated. The reported high performance towards faster hydrogenation was completed within 300 sec at 25˚C temperature and 16 sec at 60 ˚C. Synergetic behaviour of core-frame morphology provides faster electron transfer for hydrogenation and enhanced thermal stability against poisonous environment.

Keywords: Core- frame, $Ag@SiO_2NPs$, frame thickness, catalytic activity, faster reduction.

Introduction

Novel and Superior physicochemical properties of metal nanoparticles (NPs) as compared to their bulk counterparts act as a key driving force for NPs synthesis[1]. Atomic NPs consistently provide high surface property due to its large surface to volume ratio and tunable size[2]. Smaller size regime involves faster participation of NPs in surface sorption process which makes them unstable with aggregation and suffers from poisoning under the reaction conditions[3]. To terminate the particle growth reaction, the surface modification of NPs is essential. However, recent advances in the nanotechnology have led to the development of various method to form stable NPs supported with new types of stabilizers based on their application[4], Among various types of metal NPs, silver NPs (AgNPs) are recognised as interesting for the creation of novel functional materials owing to their unique optical[5], electronic[6], antibacterial[7] and catalytic features[8]. This provides the opportunity to develop the prompt AgNPs for special applications in various fields including biosensing[9], photonics[10], electronics[6], and antimicrobial activity[11]. Apart from that, AgNPs have been found to play an important role in several catalytic processes due to their distinct features like unique transition between the molecular and metallic states[12], a short range ordering with increased number of kinks, corners and edges[13]. It has been experimentally demonstrated that AgNPs have high catalytic activities towards hydrogenation[14], hydroformylation[15], carbonylation[16], etc. However, most of the catalytic reactions proceed at high temperature[17]. Under such conditions, AgNPs tends to agglomerate due to interparticle diffusion and intermolecular steric interaction between NPs. Therefore, the low thermal stability of AgNPs limits their catalytic applications inevitably and hence it is necessary to stabilize the AgNPs by embedding onto the surface of supporting materials, to suppress sintering of the metal surface[18]. Compared to single crystal Ag metal surface, the supported metal NPs attribute to complex structure in a confined state which is discrete for smaller NPs with uniform size distribution. The controlled size[19], shape[20] and dispersity of NPs play a key role in selective and enhanced catalytic activity[21]. In the recent years, preparation of supported metal NPs for a wide range of catalytic applications has been well developed[22]. Supporting can be done either by coating with polymer[23] or forming bimetallic particles[24]. The polymers used for coating from state of art like PMAPTAC-b-PDMAEMA[25], PAMAM dendrimer[26], polyguanidino oxanorbornenes[27], while in case of bimetallic part Au/Ag[28] , Ag@Fe_2O_3[29], Ag-Pt[30], Ru-Cu[31], Pt-Ir[32] were used for high catalytic activity. In bimetallic case, metal NPs were known to be highly photosensitive that leads to aggregation[33]. The resulted limitation leads to development of polymer coated AgNPs with

tremendous catalytic activity in a cheaper way. Supporting nature of polymers can control the particle size and increase the adsorption rate of the reactant over the Ag metal surface[34]. Among different polymers, silica is highly hydrophilic[35], easy to prepare, separate, optically transparent[36], easy to functionalise and label[37]. A recent report has even shown that AgNPs supported on a silica surface under ambient conditions give birth to new generation of smaller NPs in their vicinity[38]. Industrial catalyst work on the surface phenomenon which is more advantageous in silica coated AgNPs that possesses high surface[39]. This leads to more adsorption of reactant ions onto the particle surface that contributes to overcome the kinetic barrier of the reaction with less activation energy[40]. The high porous support of silica enhances the adsorption as well as surface property with high stability[41]. Surface modification of Ag@SiO_2NPs using special kind of modifiers/ stabilisers result in high rate of hydrogenation[25]. Herein, the work has been designed for faster hydrogenation by simply tweaking the morphology of AgNPs resulting in perfect quasi core-shell structure that eliminates the usage of complex modifiers. The Ag core size and SiO_2 frame thickness are expected to be tuned by the periodic variation of reactants under different reaction condition. Unlike reported methods, stabilizing agent is not required for the core – frame formation. Here, core-frame Ag@SiO_2NPs is applied as a nano-catalyst for the hydrogenation of p-nitrophenol (PNP), with an excellent catalyst activity. To the best of our knowledge, this is the first report on the use of simple quasi core –frame (Ag- SiO_2) for faster upconversion of PNP at the expense of low concentration of $NaBH_4$.

Materials

Silver Nitrate ($AgNO_3$, 99%), Cetyltrimethyl ammonium bromide (CTAB), Ascorbic acid (99%), Tetraethyl orthosilicate (TEOS, 99%), ammonium hydroxide solution (28 wt%, NH_3 in H_2O), sodium hydroxide (NaOH, 96%) were purchased from Sigma Aldrich and used without further purification. Water purified with a Milli-Q system was used throughout the experiments.

Experimental Section

Synthesis of AgNPs

AgNPs were prepared by reduction of silver nitrate using ascorbic acid that act as a reductant and CTAB as capping agent. All the glasswares were cleaned in nitric-hydrochloric acid solution for 30 min prior to use. In a typical procedure, 15 ml of 3 mM CTAB solution and 5 ml of 1mM alkaline ascorbic acid were first mixed at 25˚C temperature in an 250 ml round

bottom flask equipped with continuous stirring under 850 rpm magnetic stirring followed by the addition of 500 µl of 0.5 mM $AgNO_3$ solution in a drop wise at a rate of 6 droplets per min over a period of 10 min. The reaction was allowed to run until the solution turns into light yellow coloured solution, which indicates the monodispersed AgNPs formation.

Synthesis of core- frame Ag@SiO_2NPs through modified stober synthesis

In case of Ag@SiO_2NPs, different volume (125 µl, 250µl and 500µl in case of 1: 0.25, 1: 0.50, 1:1 volume ratio of Ag: SiO_2) of tetraethylorthosilcate (TEOS), which controls the SiO_2 thickness, was added into the above mentioned freshly prepared yellow coloured AgNPs colloids. Under continuous stirring, Silica precursor was added in dropwise for 10 min. SiO_2 thickness was easily controlled with a homogeneous coating over the entire surface of AgNPs, depending upon initial Silica precursor concentration. Later on, ammonium hydroxide solution was added over a period of 20 min for hydrolysis of Silica. The solution was kept under stirring for 24-26 h to allow formation of uniform layer of SiO_2 over the AgNPs. Upon completion of the reaction SiO_2 coated AgNPs (Ag@SiO_2NPs) were dialysed against water for 2h to separate free CTAB molecules from CTAB bound Ag@SiO_2NPs.

Catalytic hydrogenation of p-Nitrophenol

The kinetic measurement of catalytic hydrogenation of PNP was studied as a model reaction to estimate the catalytic activity of Ag@SiO_2NPs as a catalyst. The catalytic reaction was performed in a UV vis Spectrophotometer. The experiments were blanked with 1.5 ml of pure water in a quartz cuvette at room temperature. In the sample cuvette, the reaction was initiated by addition of 0.1 mM of freshly prepared PNP aqueous solution, and 3 mM of $NaBH_4$. All the reagents were thoroughly mixed for proper hydrogenation. Immediately the colour was changed from yellow to yellowish green which denotes the formation of nitrophenolate ion. Further, 0.1 nM of Ag@SiO_2NPs was added to the above solution and the time dependent absorption spectra were measured. As the hydrogenation proceeded, the bright yellow colour of the solution faded gradually and the catalytic activity was monitored. The spectral change was monitored over a scanning range of 200–700 nm at different time interval. The rate constant was calculated using the equation log ($[A_t]$/ $[A_0]$) = kt, where A_t is absorbance at time t and A_0 is absorbance at time t=0.Control experiments were carried out under identical condition that excludes the addition of Ag@SiO_2NPs. The catalytic activity of Ag@SiO_2NPs at different temperature (20- 90˚C) was studied by adopting the same procedure except the usage of spectrophotometer supplied with thermostated cell holder and the temperature was controlled by

a Peltier system (±0.1°C). For recycling the catalyst after completion of the reaction, NPs were separated by simple centrifugation and used for next cycle of the reaction described above.

Characterisation

The morphology of the AgNPs and Ag@SiO_2NPs was investigated by high-resolution TEM (HR-TEM; JEOL 3010 electron microscope at the accelerating voltage of 200 kV) and SEM-EDAX of Ag@SiO_2NPs was performed with a Hitachi-SU6600 operating at 15.0 kV. Dynamic Light Scattering (DLS) was performed on a Zetasizer Nano ZS using 4 mW He/Ne laser (632.8 nm wavelength) with scattering angle of 175˚. The solution of AgNPs and Ag@SiO_2NPs were subjected to filtration using PTFE 0.45 μm before DLS measurements. The obtained particle size was an average of five separate measurements, and the measurement uncertainty was indicated as standard deviation. A quartz cuvette with 1-cm optical path length was used. Fourier transform infrared (FTIR) spectra were recorded on ABBMB 3000 Fourier transform infra-red (FTIR) spectrophotometer in the region 4000 to 6000 cm^{-1} over KBr pressed pellets. The thermogravimetry analysis (TGA) of the samples was performed using a Q50 TA instrument from 25 to 900 °C in an air flow at a heating rate of 5 °C min^{-1}. TA instruments Universal analysis 2000 software was used for data acquisition and processing. All UV-vis absorption Spectra of samples were recorded on a Perkin Elmer Lamba 35 spectrophotometer supplied with thermostatted cell holder. The temperature was controlled by a Peltier system (±0.1 °C).

Result and discussion

A simple versatile procedure has been developed to form the core-frame structure of Ag@SiO_2NPs without any prior modification of AgNPs using complex additives like dendrimers, modifiers at room temperature and pressure in aqueous solution. Therefore, the modified synthetic procedure reported here provides Silica coated AgNPs with controlled shape and size distribution. The outer protective layer of SiO_2 frame not only enhances the stability of AgNPs by hindering AgNPs interaction with outer poisonous environment but also prevents direct interaction which avoids agglomeration of AgNPs. The schematic illustration of synthesis of hybrid Ag@SiO_2NPs with different frame thickness is shown in the Fig. 1. AgNPs was embedded into different SiO_2 frame thickness which was controlled by volume ratio of Ag and Silica. The AgNPs and quasi core-frame Ag@SiO_2NPs were characterized by various techniques, which is summarised below.

The surface morphology, aggregation state, and the particle size of AgNPs and Ag@SiO_2NPs with different frame thickness were investigated by Transmission electron microscope (TEM) as shown in Fig. 2(a-d). Figure 2a shows the TEM image of AgNPs formed with average diameter of 35 nm. By varying the volume ratio between the Silica precursor and Ag core, the frame thickness over the AgNPs were frabicated resulting in the formation of stable Ag@SiO_2NPs with controlled morphology. The thickness of the SiO_2 frame was 2 nm (Fig b), 5 nm (Fig c), and 14 nm(Fig d), respectively in the case of 1: 0.25, 1: 0.50, 1:1 volume ratio of Ag: SiO_2. The lower frame thickness of SiO_2 (Fig b and c) divulge that AgNPs aggregated prior to the SiO_2 shell formation due to the lesser number of TEOS molecules in the presence of high ionic strength medium. This induces the faster hydrolysis of TEOS which leads to thin SiO_2 frame formation over AgNPs rather than core – frame[42]. However, at volume ratio of 1:1, Ag@SiO_2 NPs forms monodispersed NPs with an average diameter of 30 nm though the particles have multiple core. The formed Ag@SiO_2NPs resembles the typical quasi perfect core–frame structure with 9 nm Ag core, seen as darker shade of gray which was embedded into the 12 nm thick nano SiO_2 frame visible as a lighter region. Therefore, it is apparent that nanoscale frame are uniformly distributed all over the surfaces of AgNPs and the particle surface becomes increasingly textured as the frame thickness increases progressively. Further, the hydrodynamic distributions of core-frame morphology of Ag@SiO_2NPs shown in Fig. 3 indicate that the samples were highly monodispersed with narrow size distributions typically with a standard deviation of less than 2% (based on average of 100 particles).. The average hydrodynamic diameter of the AgNPs were 50 nm while in the case of Ag@SiO_2NPs they showed increment of 15 nm in size range indicating the additional SiO_2 frame formation which was confirmed earlier in TEM results. Consequently, it confirms that SiO_2 was coated legitimately over the surface of AgNPs in a single step polymerisation. Moreover, the presence of SiO_2 frame was confirmed by SEM-EDX measurement of Ag@SiO_2NPs in Fig. (4 (a) & (b)). The SEM image inferred that the particles were tightly packed as identical spheres. The quantitative estimation of spheres clearly proves the existence of elements like Ag, Si and O. The precise size control and formation of stable perfect Core- frame morphology was confirmed by microscopic studies. It is worth noting that the SiO_2 frame distributed homogeneously on each individual AgNPs with no free particles and it would appear that all the AgNPs stay intact upon surface coating by SiO_2NPs.

The Surface Plasmon Resonance of NPs from UV–Visible extinction spectrum is a systematic and prevalent method to know the state of NPs in solution. The excitation spectra of freshly

prepared AgNPs solution showed a strong maximum excitation peak at 400 nm (Fig. 5), which characterises the collective excitation of the free conduction band electrons of the NPs, known as the Surface Plasmon Resonance (SPR)[43]. Here we have characterised the impact of supported nano SiO_2 over the AgNPs from SPR band of AgNPs as shown in Fig. 5. In general, the formation of a dielectric layer around a metallic NPs results in a shift of the SPR to lower energies (longer wavelengths) and an increase in the extinction coefficient. It can be seen from Fig. 5. That the excitation maximum observed for AgNPs at 400 nm is shifted to 409 nm in Ag@SiO_2NPs. This clearly indicates that formation of SiO_2 layers around the AgNPs in this case of Ag@SiO_2NPs. The spectra revealed that the excitation maximum of Ag@SiO_2NPs at 400 nm favours bathochromic shift to 409 nm, which corresponds to exchange of CTAB molecules between the metal surface and polymeric SiO_2 frame. This shift correlates directly with the dielectric constant of the medium[44] and increase in the local refractive index around the NPs[45]. The sharp excitation peak indicates the high resistivity of NPs aggregation.

Further, excitation spectra of prepared Ag NPs and NPs supported SiO_2 frame were measured over a period of months to monitor the stability of NPs. Both AgNPs and Ag@SiO_2NPs appeared to be invariant in their maximum excitation shift except quick reduction in absorbance of AgNPs as shown in the Fig. 6. The AgNPs introduces continuous decrease in their maximum absorbance within 60 days, but the Ag@SiO_2NPs showed stabilised nature even after 120 days by minimal change in corresponding absorbance. This clearly exhibit that polymeric SiO_2 frame serve as a protective layer, which effectively prevent aggregation caused by the steric interaction between the AgNPs[46]. The chemically inert nature of SiO_2 frame over the metal AgNPs limits photooxidation by providing them high stability against light over a long period of time shown in the Fig. 7. Further, the stability was confirmed by visual assessment shown in Fig. 8. The yellow colored AgNPs diminishes rapidly into colourless solution due to high photooxidation rate. In sharp contrast, the Ag@SiO_2NPs maintains a stable excitation and could maintain distinctive yellow colour (indication of monodispersed AgNPs) even after the six month period. The low photostability of AgNPs significantly limits their practical applications by turning into colourless solution, which was not discerned in AgNPs supported SiO_2 frame due to the high stability of AgNPs provided by SiO_2 frame.

The thermal stability of AgNPs by SiO_2 frame in Ag@SiO_2NPs was investigated by thermogravimetry analysis and their excitation measurement. The analysis was carried out to investigate the effect of SiO_2 coating on stability of AgNPs and their corresponding organic residues. Fig. 9 showed the weight loss profile of the AgNPs and Ag@SiO_2NPs during heating

from 25 to 900 ˚C at an increment of 5 ˚C min^{-1}.The TGA curves of the AgNPs differ from that of Ag@SiO_2NPs with low mass percentage at 900 ˚C. The first weight loss of AgNPs observed at 200 to 280 ˚C is attributed to degradation of attached stabiliser CTAB molecules [47] over the AgNPs. The weight loss was increased and reached 80% at 290 ˚C and upto 95% at 800 ˚C. Similarly, TGA curve of Ag@SiO_2NPs (Fig 9) showed that the degradation occurred in two distinct regions. The first weight loss from 208 to 280 ˚C with 60% mass was due to thermodesorption of water and organic components[48] . The reduction in weight demands an understanding the nature of thermally desorbed species on the surface of SiO_2 spheres[49]. The surface of spherical SiO_2 ultimately contains very small portion of free silanols, a large amount of hydrogen bonded silanols, and adsorbed water molecules[50]. The silanols and water molecules can be populated on the outer spherical surface of the particles, as well as on the inner pore walls[51]. The second degradation occurred at 280 to 700 ˚C with 10% weight loss which can be associated with desorption of adsorbed water present in the both outer as well as inner walls of SiO_2[52]. The difference in the weight percentage of the Ag@SiO_2NPs with different shell thickness of silica was analysed and presented in the Fig. 9. A substantial amount of mass was present at 900 °C which could be assigned to the AgNPs. These results are in good agreement with previously published results[53]. This difference in weight loss of AgNPs and Ag@SiO_2NPs with different shell thickness was believed to be due to the presence of more organic molecules over the AgNPs which undergo faster degradation at low temperature. In contrast, Ag@SiO_2NPs was predominantly surrounded by inorganic molecules which showed less reduction in weight loss even at high temperature. Therefore, the enhanced thermal stability of composite Ag@SiO_2NPs was observed due to the presence of stable inorganic SiO_2 frame over the AgNPs. The stability of AgNPs and Ag@SiO_2NPs was also analysed by subjecting NPs to various temperature from 20 to 90 ˚C in Peltier system chamber (keeping other parameters constant) and the corresponding excitation spectra was recorded. The maximum excitation peak demonstrate that AgNPs supported into SiO_2 frame do not discern any shift in their maximum excitation which indicated the stabilization of AgNPs by polymeric SiO_2 frame [17] even at higher temperature (Fig. 10 (a and b)). The minimum changes in their spectra demonstrate NPs stability in hybrid state. While in the case of AgNPs, they have undergone continuous decrease in their maximum excitation due to the direct exposure of metal surface to outer environment.

The functionality of polymeric SiO_2 frame over the AgNPs was investigated by Fourier transform Infrared Spectroscopy and the spectrum is shown in Fig. 11. The AgNPs showed the characteristic band at 3018 cm^{-1} which correspond to the C-H stretching of CTAB[54]. The sharp

absorption band at 2921 cm^{-1} and 2848 cm^{-1} is attributed to CH_3 anti symmetric stretching and CH_3 adjacent to Nitrogen respectively. The IR pattern of AgNPs was very similar to that of Ag@SiO_2NPs except the broad signals at 989- 1286 cm^{-1} which corresponds to Si bonding [55,20]. However, the close inspection of AgNPs spectra showed that small protrusion near 3018 cm^{-1} indicate the CH_2 stretching near the positive charge of AgNPs. As discussed earlier, AgNPs supported on polymeric Silica frame showed insertion at 989- 1286 cm^{-1} region which is attributed to the presence of polymeric SiO_2 on the composite. In general, a very strong and broad IR signals at 1047 cm^{-1} with a shoulder at 1130 cm^{-1} was assigned to the transverse-optical (TO) and longitudinal-optical (LO) modes of the Si–O–Si asymmetric stretching vibrations, respectively [56]. The slight shift and broadening of these band to 1074 cm^{-1} and 1226 cm^{-1} indicated the Si-O-Ag bond formation which was absent in the AgNPs. It may relevant to discussion that the symmetric and asymmetric stretching frequencies of functional group undergo a blue shift, due to the confinement arising from the outer polymeric cage[57]. The absorption band at 3422 cm^{-1} in the polymeric Si was due to the stretching vibrations of Si–OH groups[7, 58] of polymeric SiO_2 frame. The absorption band at 795 cm^{-1} could be associated with the Si–O–Si symmetric stretching vibrations of Si[59]. At the same time increase in the intensity of band at 3422 cm^{-1} showed the presence of more number of hydroxyl groups indicates the presence of hydroxyl ions over the AgNPs. These results clearly demonstrate that the AgNPs were confined inside the polymeric SiO_2 through hydrogen bonding and the absence of free Si band disclosed that all AgNPs effectively embedded inside the SiO_2 frame.

Rocket fire reduction of Nitrophenol by Ag@SiO_2NPs as a substrate

On the whole, observation concludes the uniform loading of 5- 12 nm sized AgNPs (1:1 volume ratio of Ag: Si) on the nano SiO_2 frame possess high stability. The catalytic performance of Ag@SiO_2NPs was determined by evaluating the kinetics of the catalytic hydrogenation of PNP. The Ag@SiO_2NPs was found to be stable in aqueous solution hence the catalytic reduction of PNP was carried out in water medium[60]. The UV-vis absorption spectroscopy was used to monitor the reduction kinetics of PNP in the presence and absence of both catalysts AgNPs and Ag@SiO_2NPs under the same experimental condition as shown in Fig. 12. Upon addition of AgNPs to the reaction mixture (PNP and borohydride) at 25˚C temperature, the absorption peak at 400 nm remain unaltered for a long period, which implies that nitrophenolate anions were not readily reduced by aqueous $NaBH_4$ (Fig. 12 B) [61]. On the other hand, in the presence of a small amount of Ag@SiO_2NPs catalyst, fading and ultimate bleaching of greenish- yellow colour of

nitrophenolate ion in the solution was observed within 300 sec as shown in Fig 12 (C), which indicates the progress of

S.no	Composite NPs formulation	$NaBH_4$ input (M)	Reaction time (sec) @ room temperature	Rate constant	Modifier /stabiliser
1	Ni core –Si shell	0.2	960	2.818×10^{-3} s^{-1}	EDTA [62]
2	NAP-Mg–Au(0)	0.01	150	7.6×10^{-3} s^{-1}	[63]
3	$Ag@SiO_2$	0.01	720	0.37 min^{-1}	PMAPTACb-PDMAEMA [25]
4	Ni NPs	0.2	Above 600	2.7×10^{-3} s^{-1}	CTAB, PEG-10000, gelatin [64]
5	Au(0)@TpPa-1	-	780	5.35×10^{-3} s^{-1}	TpPa-1 [65]
6	Dendrimer-Silver Nanocomposites	0.03	-	$5.9x\ 10^{-4}$ s^{-1}	poly(amido)amine dendrimers [26]
7	Fe3O4@SN/HPW@CG–Ag	0.2	420	0.53 min^{-1}	chitosan[66]
8	Nickel NPs	0.01	-	1×10^{-3} s^{-1}	spherical poly (acrylic acid) (PAA) brushes[67]
9	$Au\text{-}Fe_3O_4$	0.1	600	0.72 min^{-1}	oleate[68]
10	Fe_3O_4@PBLG@Au NPs	-	1620	-	poly(γ-benzyl-L-glutamate)[69]
11	$G4\text{-}NH_2(Pd_x)$ DENs	0.2	-	5.82×10^{-3} s^{-1}	poly(amido)amine (PAMAM) dendrimer[70]
12	Ni/graphene NPs	0.132	Above 300	11.7×10^{-3} s^{-1}	-[22]
13	PPI dendrimer-palladium	0.03	720	-	PPI dendrimer[26]
15	AgNP-PA-3K	0.012	660	5.50×10^{-3} s^{-1}	polyamino oxanorbornenes[27]
16	Ag@Nanosilica		2400	5.35×10^{-3} s^{-1}	Rhizopus oryzae[71]
17	Au/Ag	0.015	150	-	DPS[24]
18	AuNP−CNT	0.1	-	62 μms^{-1}	CNT[72]
19	Au@ ESm	-	420	6.3×10^{-3} s^{-1}	ESm[73]
20	CD -AgNPs	0.007	1260	1.94×10^{-3} s^{-1}	Cyclodextrin[74]

PNP reduction. As the reaction proceeds, the absorbance of PNP at 400 nm started to decrease with simultaneous increase in absorbance at 300 nm corresponding to the formation of 4-aminoPhenol. Furthermore, the time required for the reduction was less than that reported previously with hybrid Silica coated catalysts. The reduction time with different catalyst concentration were presented in the table 1.From the table, it can be seen that the time taken for hydrogenation of PNP was reduced to greater extent while using porous carrier Ag@SiO_2NPs as catalyst. The probable reason for the momentous activity shown by Ag@SiO_2NPs is due to the fine distribution of very tiny NPs (5 - 12 nm) into porous SiO_2 matrix, which lead to a very large surface area of the NPs and high particle number per unit mass for the catalyst[75]. The increased fraction of the atoms at the surface of Ag@SiO_2NPs leads to higher catalytic activity[76]. It has been reported that the larger regular sphere possess higher catalytic activity due to more number of permeable perpendicular pore channels of porous silica [77]. This could be attributed to the high degree of exposure of surface active sites in spherical morphology. In hydrogenation, the unpaired electrons could work with PNP, which is the adsorbate, to form an adsorption bond with the catalyst [64].Here, the attractive interactions of substrate with protective polymer SiO_2 frame result in higher hydrogenation rate. On the other hand, the porous SiO_2 in colloidal dispersion of Ag@SiO_2NPs enhance the faster electron transfer and also it can shield deactivation of AgNPs from catalytic poison or air[40]. The catalytic activity of Ag@ porous SiO_2 as a catalyst showed faster rate of reduction obtained from synergetic effect of stable high surface area of AgNPs with faster adsorption of reactants over porous SiO_2 matrices[39]. Similarly, the catalytic activity of Ag@SiO_2NPs in the presence of various temperatures was studied and shown in Fig. 13.

For the first time, we have reported the faster hydrogenation of PNP within a fraction of second (16 Sec) at high temperature (60 ˚C) as shown in Fig. 12 (D) without the addition of any stabilisers to the reaction medium. This was attributed to the swelling nature of porous SiO_2 which increases the adsorption rate of nitrophenolate ion at high temperature[78]. This suggests that the reaction is favourable at higher temperature due to the more adsorption of the reactant on the catalyst surface, which plays an important role in activating the reaction process. To measure the catalytic performance of these catalysts, rate constant has been determined from the Pseudo-First order kinetics (Fig. 14 (a and b)). The linear correlation of log (A/A_0) versus time (s) at any instant was obtained. Compared to prior art rate constant values in table 1, our system showed the catalytic activity with rate constant of 6.5×10^{-3} s^{-1} (correlation coefficient of $R^2 = 0.99$). The high catalytic activity and rate constant is attributed to the following reasons. Primarily, the

AgNPs are formed as uniform spherical spheres in a monodispersed form, its smaller size showed the high surface area to volume which is responsible for high absorption of nitrophenolate ions. Secondly, the protective porous SiO_2 frame protects the inner metal from poisonous air and improved their stability and reusability for upto 7 cycles. On the other hand, faster photo activity of AgNPs towards the light induces particle aggregation and limits their reusability. Thirdly, fine coating of SiO_2NPs greatly improved the electron transfer between the substrate and the reactant. On the whole the synergetic effect of smaller Ag metal with high adsorption of substrate over the SiO_2 frame showed the very effective catalytic activity at faster rate without any additional chemical additives. Further the reusability of the catalyst Ag@SiO_2NPs was studied. After completion of the hydrogenation, Ag@SiO_2NPs was separated from the mixture by centrifugation with 12000 rpm for 20 min, and the pellet was washed with deionized water. Then the recovered catalyst was reused in the next cycle of the reaction. This procedure was repeated for 8 times after the seventh cycle there is decrease in the conversion efficiency (Fig 15) indicate that the Ag@SiO_2NPs showed significant catalytic activity upto seven cycles of reaction.

Conclusions

The quasi perfect core–frame structure was perfectly fabricated by amendment in the reactant input like volume ratio of Ag and SiO2 without any prior modification of AgNPs. The geometry dependent morphology of core-frame hybrid Ag@SiO_2NPs was thoroughly investigated through different experimental techniques. The behaviour of Ag@SiO_2NPs towards optical and thermal treatment clearly demonstrates the core-frame formation along with their stability against aggregation and poisonous environments. The controlled tuning of frame thickness with high stability provides unique opportunity to employ this core-frame hybrid Ag@SiO_2NPs as a catalyst for hydrogenation of PNP at a faster rate in different temperature. The kinetic studies of hydrogenation revealed that the synthesized Ag@SiO_2NPs exhibited a faster activity by completing the hydrogenation within 300 sec at 25˚C temperature and 16 sec at 60 ˚C. Moreover, these results suggest that the Ag@SiO_2NPs act as a platform for the synthesis of economic core - frame catalyst in a simplest way.

References

1. J. M. Campelo, D. Luna, R. Luque, J. M. Marinas and A. A. Romero, *ChemSusChem*, 2009, 2, 18-45.
2. R. J. White, R. Luque, V. L. Budarin, J. H. Clark and D. J. Macquarrie, *Chem. Soc. Rev*, 2009, 38, 481-494.
3. C. A. Mirkin, *Small*, 2005, 1, 14-16.
4. R. Ghosh Chaudhuri and S. Paria, *Chem. Rev.*, 2012, 112, 2373-2433.
5. J. B. Jackson and N. J. Halas, *J. Phys. Chem. A*, 2001, 105, 2743-2746.
6. Y. Li, Y. Wu and B. S. Ong, *J. Am. Chem. Soc*, 2005, 127, 3266-3267.
7. J. Song, H. Kim, Y. Jang and J. Jang, *ACS Appl. Mater. Interfaces*, 2013, 5, 11563-11568.
8. A. C. Patel, S. Li, C. Wang, W. Zhang and Y. Wei, *Chem. Mater.*, 2007, 19, 1231-1238.
9. S. Sahoo, S. Husale, S. Karna, S. K. Nayak and P. M. Ajayan, *J. Am. Chem. Soc*, 2011, 133, 4005-4009.
10. M. Mitsuishi, H. Tanaka, M. Obata and T. Miyashita, *Langmuir*, 2010, 26, 15117-15120.
11. D. M. Eby, N. M. Schaeublin, K. E. Farrington, S. M. Hussain and G. R. Johnson, *ACS Nano*, 2009, 3, 984-994.
12. D. Radziuk, D. G. Shchukin, A. Skirtach, H. Möhwald and G. Sukhorukov, *Langmuir*, 2007, 23, 4612-4617.
13. D. M. Popolan, No, R. Mitric, T. M. Bernhardt and V. Bonacic-Koutecky, *Phys. Chem. Chem. Phys.*, 2010, 12, 7865-7873.
14. Q. Luo, T. Wang, M. Beller and H. Jiao, *J. Phys. Chem. C*, 2013, 117, 12715-12724.
15. W. K. Wilmarth and A. F. Kapauan, *J. Am. Chem. Soc*, 1956, 78, 1308-1311.
16. T. Verano-Braga, R. Miethling-Graff, K. Wojdyla, A. Rogowska-Wrzesinska, J. R. Brewer, H. Erdmann and F. Kjeldsen, *ACS Nano*, 2014, 8, 2161-2175.
17. J. Sun, D. Ma, H. Zhang, X. Liu, X. Han, X. Bao, G. Weinberg, N. Pfänder and D. Su, *J. Am. Chem. Soc*, 2006, 128, 15756-15764.
18. C.-J. Jia and F. Schuth, *Phys. Chem. Chem. Phys.*, 2011, 13, 2457-2487.
19. R. W. Murray, *Chem. Rev.*, 2008, 108, 2688-2720.
20. B. Tang, J. Li, X. Hou, T. Afrin, L. Sun and X. Wang, *Ind. Eng. Chem. Res.*, 2013, 52, 4556-4563.
21. W. Schartl, *Nanoscale*, 2010, 2, 829-843.
22. Y.-g. Wu, M. Wen, Q.-s. Wu and H. Fang, *J. Phys. Chem. C*, 2014, 118, 6307-6313.
23. S. Nam, H. W. Cho, S. Lim, D. Kim, H. Kim and B. J. Sung, *ACS Nano*, 2012, 7, 851-856.
24. B. Xia, F. He and L. Li, *Langmuir*, 2013, 29, 4901-4907.
25. B. P. Bastakoti, S. Guragain, S.-i. Yusa and K. Nakashima, *RSC Adv.*, 2012, 2, 5938-5940.
26. K. Esumi, R. Isono and T. Yoshimura, *Langmuir*, 2004, 20, 237-243.
27. B. Baruah, G. J. Gabriel, M. J. Akbashev and M. E. Booher, *Langmuir*, 2013, 29, 4225-4234.
28. J.-H. Liu, A.-Q. Wang, Y.-S. Chi, H.-P. Lin and C.-Y. Mou, *J. Phys. Chem. B*, 2004, 109, 40-43.
29. G. Li and Z. Tang, *Nanoscale*, 2014, 6, 3995-4011.

30. C.-L. Lee and C.-M. Tseng, *J. Phys. Chem. C*, 2008, 112, 13342-13345.
31. A. J. Hong, A. J. Rouco, D. E. Resasco and G. L. Haller, *J. Phys. Chem.* 1987, 91, 2665-2671.
32. A. Charron, C. Kappenstein, M. Guerin and Z. Paal, *Phys. Chem. Chem. Phys.*, 1999, 1, 3817-3822.
33. X. Zhang, H. Wang and Z. Su, *Langmuir*, 2012, 28, 15705-15712.
34. J. Pecher and S. Mecking, *Chem. Rev.*, 2010, 110, 6260-6279.
35. M. Nakamura, M. Shono and K. Ishimura, *Anal. Chem.*, 2007, 79, 6507-6514.
36. M. Qhobosheane, S. Santra, P. Zhang and W. Tan, *Analyst*, 2001, 126, 1274-1278.
37. M. T. Hurley, Z. Wang, A. Mahle, D. Rabin, Q. Liu, D. S. English, M. R. Zachariah, D. Stein and P. DeShong, *Adv. Funct. Mater.*, 2013, 23, 3335-3343.
38. M. Agrawal, S. Gupta and M. Stamm, *J. Mater. Chem.*, 2011, 21, 615-627.
39. Z.-J. Jiang, C.-Y. Liu and L.-W. Sun, *J. Phys. Chem. B*, 2005, 109, 1730-1735.
40. Z. Deng, M. Chen and L. Wu, *J. Phys. Chem. C*, 2007, 111, 11692-11698.
41. R. Kumar, I. Roy, T. Y. Ohulchanskyy, L. N. Goswami, A. C. Bonoiu, E. J. Bergey, K. M. Tramposch, A. Maitra and P. N. Prasad, *ACS Nano*, 2008, 2, 449-456.
42. Y. Jiao, J. Guo, S. Shen, B. Chang, Y. Zhang, X. Jiang and W. Yang, *J. Mater. Chem.*, 2012, 22, 17636-17643.
43. B. Khlebtsov and N. Khlebtsov, *biomedo.*, 2006, 11, 044002-044002-044005.
44. M. M. Y. Chen and A. Katz, *Langmuir*, 2002, 18, 8566-8572.
45. L. M. Liz-Marzán, M. Giersig and P. Mulvaney, *Langmuir*, 1996, 12, 4329-4335.
46. L.-W. Jang, D.-W. Jeon, M. Kim, J.-W. Jeon, A. Y. Polyakov, J.-W. Ju, S.-J. Lee, J.-H. Baek, J.-K. Yang and I.-H. Lee, *Adv. Funct. Mater.*, 2012, 22, 2728-2734.
47. Z. Sui, X. Chen, L. Wang, Y. Chai, C. Yang and J. Zhao, *Chem. Lett.*, 2005, 34, 100-101.
48. C. P. Jaroniec, R. K. Gilpin and M. Jaroniec, *J. Phys. Chem. B,* 1997, 101, 6861-6866.
49. V. G. Pol, D. N. Srivastava, O. Palchik, V. Palchik, M. A. Slifkin, A. M. Weiss and A. Gedanken, *Langmuir*, 2002, 18, 3352-3357.
50. S. Ramesh, Y. Cohen, R. Prozorov, K. V. P. M. Shafi, D. Aurbach and A. Gedanken, *J. Phys. Chem. B*, 1998, 102, 10234-10242.
51. H. Zou, R. Wang, X. Li, X. Wang, S. Zeng, S. Ding, L. Li, Z. Zhang and S. Qiu, *J. Mater. Chem. A,* 2014, 2, 12403-12412.
52. U. Shinichi, N. Kazuo, M. Satoru and M. Mizuho, *Jpn. J. Appl. Phys.*, 2004, 43, 8242.
53. V. G. Pol, A. Gedanken and J. Calderon-Moreno, *Chem. Mater.*, 2003, 15, 1111-1118.
54. L. Huang, X. Chen and Q. Li, *J. Mater. Chem.*, 2001, 11, 610-615.
55. B. Tang, M. Zhang, X. Hou, J. Li, L. Sun and X. Wang, *Ind. Eng. Chem. Res.*, 2012, 51, 12807-12813.
56. P. Innocenzi, *J. Non-Cryst. Solids*, 2003, 316, 309-319.
57. O. Shameema, C. N. Ramachandran and N. Sathyamurthy, *J. Phys. Chem. A*, 2005, 110, 2-4.
58. B. Sahoo, K. S. P. Devi, S. K. Sahu, S. Nayak, T. K. Maiti, D. Dhara and P. Pramanik, *Biomater. Sci.*, 2013, 1, 647-657.
59. J.-D. Brassard, D. K. Sarkar and J. Perron, *ACS Appl. Mater. Interfaces*, 2011, 3, 3583-3588.
60. M. L. Farré, A. Oubiña, M. P. Marco, A. Ginebreda, L. Tirapu and D. Barceló, *Environ. Sci. Technol.*, 1999, 33, 3898-3904.
61. Z. Niu, Q. Peng, M. Gong, H. Rong and Y. Li, *Angewandte Chemie International Edition*, 2011, 50, 6315-6319.
62. Z. Jiang, J. Xie, D. Jiang, J. Jing and H. Qin, *CrystEngComm*, 2012, 14, 4601-4611.
63. K. Layek, M. L. Kantam, M. Shirai, D. Nishio-Hamane, T. Sasaki and H. Maheswaran, *Green Chem.*, 2012, 14, 3164-3174.

64. Z. Jiang, J. Xie, D. Jiang, X. Wei and M. Chen, *CrystEngComm*, 2013, 15, 560-569.
65. P. Pachfule, S. Kandambeth, D. Diaz Diaz and R. Banerjee, *Chem. Commun.*, 2014, 50, 3169-3172.
66. Z. Wang, S. Zhai, B. Zhai, Z. Xiao, F. Zhang and Q. An, *New J. Chem.*, 2014, 38, 3999-4006.
67. Z. Zhu, X. Guo, S. Wu, R. Zhang, J. Wang and L. Li, *Ind. Eng. Chem. Res.*, 2011, 50, 13848-13853.
68. F.-h. Lin and R.-a. Doong, *J. Phys. Chem. C,* 2011, 115, 6591-6598.
69. G. Marcelo, A. Muñoz-Bonilla and M. Fernández-García, *J. Phys. Chem. C*, 2012, 116, 24717-24725.
70. J. A. Johnson, J. J. Makis, K. A. Marvin, S. E. Rodenbusch and K. J. Stevenson, *J. Phys. Chem. C*, 2013, 117, 22644-22651.
71. S. K. Das, M. M. R. Khan, A. K. Guha and N. Naskar, *Green Chem.*, 2013, 15, 2548-2557.
72. H. Wang, Z. Dong and C. Na, *ACS Sustainable Chem. Eng.*, 2013, 1, 746-752.
73. R. Mallampati and S. Valiyaveettil, *ACS Sustainable Chem. Eng.*, 2014, 2, 855-859.
74. L. B. Devi and A. B. Mandal, *RSC Adv.***,** 2013, 3, 5238-5253.
75. B. Hvolbæk, T. V. W. Janssens, B. S. Clausen, H. Falsig, C. H. Christensen and J. K. Nørskov, *Nano Today*, 2007, 2, 14-18.
76. E. Roduner, *Chem. Soc. Rev.*, 2006, 35, 583-592.
77. X. Fang, Z. Liu, M.-F. Hsieh, M. Chen, P. Liu, C. Chen and N. Zheng, *ACS Nano*, 2012, 6, 4434-4444.
78. B. Schmitz, U. Müller, N. Trukhan, M. Schubert, G. Férey and M. Hirscher, *ChemPhysChem*, 2008, 9, 2181-2184.

Figure Captions

Figure 1 Schematic illustration for the preparation of hybrid Ag@SiO_2NPs with different frame thickness.

Figure 2 HRTEM image of (a) AgNPs without SiO_2 coating , (b) dispersed AgNPs confined in 2 nm SiO_2 frame, (c) dispersed AgNPs confined in 5 nm SiO_2 frame, and (d) quasi perfect core frame Ag@SiO_2 NPs, the diameter of Ag core 8 nm and SiO_2 frame thickness 15 nm: (a-d) denotes magnification at 100nm and (a_1-d_1) denotes magification at 10 nm.

Figure 3 Hydrodynamic radius of the (a) dispersed AgNPs and (b) Monodispersed Ag@SiO_2NPs.

Figure 4 (a) SEM and (b) EDAX of Ag@SiO_2NPs.

Figure 5 Absorption spectrum of a suspension of Ag and Ag@SiO_2NPs dispersed in water with the plasmon peak centered at 400 nm and 409 nm (red indicates AgNPs and Black indicates Ag@SiO_2NPs)

Figure 6 UV-Visible spectra of (A) AgNPs with Plasmon peak centred at 400 nm, black line indicate 0^{th} day and orange line indicate 60^{th} day old solution, (B) Ag@SiO_2NPs with Plasmon peak centred at 409 nm, Black line indicate 0^{th} day solution and Blue line indicate 120^{th} day.

Figure 7 The proposed mechanism for the nucleation and stabilisation of NPs (AgNPs and Ag@SiO_2NPs) at different time periods.

Figure 8 The Visual assessment of stability of NPs over theperiod of time 1) Ag@SiO_2NPs and 2) AgNPs in which (A - F) denotes the different time period from 1^{st} day to 120^{th} day old solution.

Figure 9 Thermogravimetry analysis of both AgNPs and Ag@SiO_2NPs (different shell thickness of silica). The Black line indicates 1:1 ratio of Ag: SiO_2, blue indicates 1:0.5 ratio of Ag: SiO_2, red indicates 1:0.25 ratio of Ag: SiO_2, and green indicates AgNPs.

Figure 10 (a) Changes in the maximum absorbance of AgNPs and Ag@SiO_2NPs at different temperature from (20˚C to 90˚C) and (b) UV-Visible spectra of (1) AgNPs and (2) Ag@SiO_2NPs at different temperature from (20˚C to 90˚C)

Figure 11 FT-IR spectra of Ag and Ag@SiO_2NPs.

Figure 12 Time dependent UV-Vis absorption spectra for the hydrogenation of PNP to 4-Aminophenol, with and without catalyst (A) in the absence of catalyst at 25˚C, (B) in the presence of AgNPs as a catalyst at 25˚C, (C) in the presence of Ag@SiO_2NPs as a catalyst at 25˚C and (D) Ag@SiO_2NPs as a catalyst at 60˚C.

Figure 13 Plot of the absorbance of PNP at 400 nm versus time for the reduction of PNP catalyzed by AgSiO_2NPs and AgNPs.

Figure 14 (a) The change in the maximum excitation for p-nitrophenol as a function of time at different temperature and (b) In (A_0/A_t) versus time for the AgSiO_2NPs catalytic reduction of PNP.

Figure 15 Reusability of the AgSiO_2NPs catalyst for the hydrogenation of PNP to 4-Aminophenol.

Table 1 Comparison of rate constants and time of completion of p-nitrophenol reduction using different NPs as substrate

Figure 1

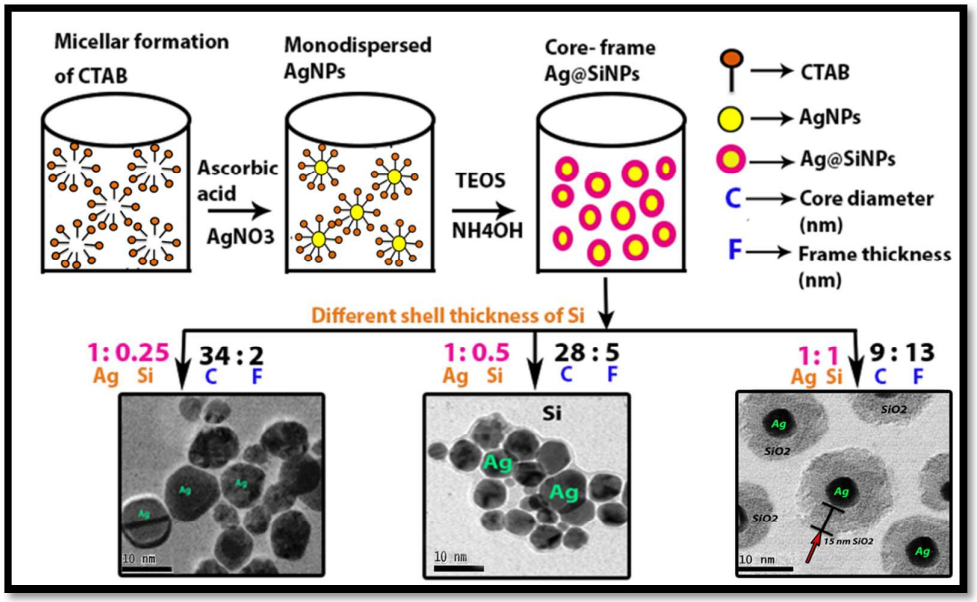
Micellar formation of CTAB
Monodispersed AgNPs
Core- frame Ag@SiNPs
Ascorbic acid
AgNO3
TEOS
NH4OH
CTAB
AgNPs
Ag@SiNPs
C Core diameter (nm)
F Frame thickness (nm)
Different shell thickness of Si
1: 0.25 Ag Si
34 : 2 C F
1: 0.5 Ag Si
28 : 5 C F
1: 1 Ag Si
9 : 13 C F
Si
Ag
SiO2
10 nm
15 nm SiO2

Figure 2

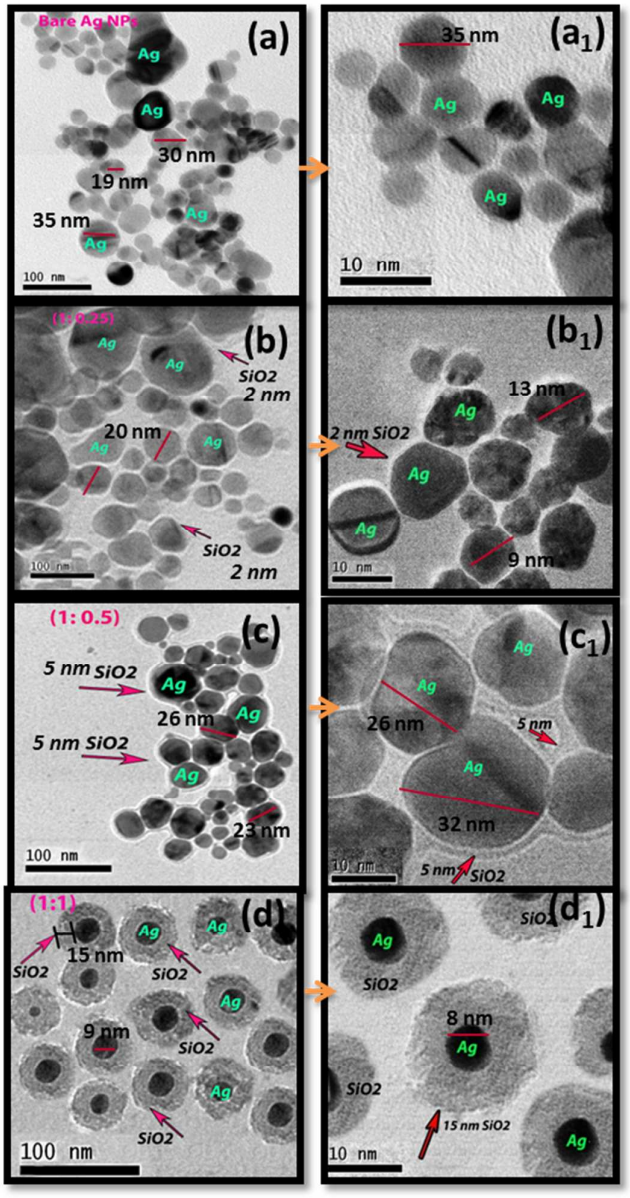
Bare Ag NPs
(a)
Ag
30 nm
19 nm
35 nm
100 nm
(a1)
35 nm
10 nm
(1: 0.25)
(b)
SiO2
2 nm
20 nm
100 nm
(b1)
13 nm
2 nm SiO2
9 nm
10 nm
(1: 0.5)
(c)
5 nm SiO2
26 nm
23 nm
100 nm
(c1)
32 nm
5 nm
(1:1)
(d)
15 nm
9 nm
100 nm
(d1)
8 nm
15 nm SiO2
10 nm

Figure 3

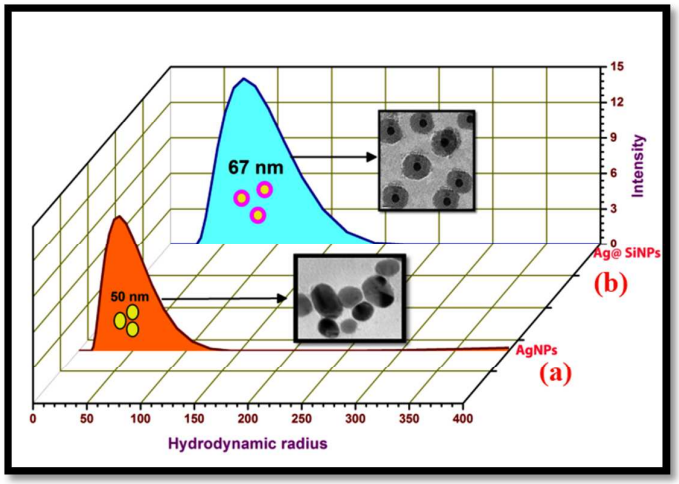
67 nm
50 nm
Intensity
15
12
9
6
3
0
Ag@ SiNPs
(b)
AgNPs
(a)
0
50
100
150
200
250
300
350
400
Hydrodynamic radius

Figure 4

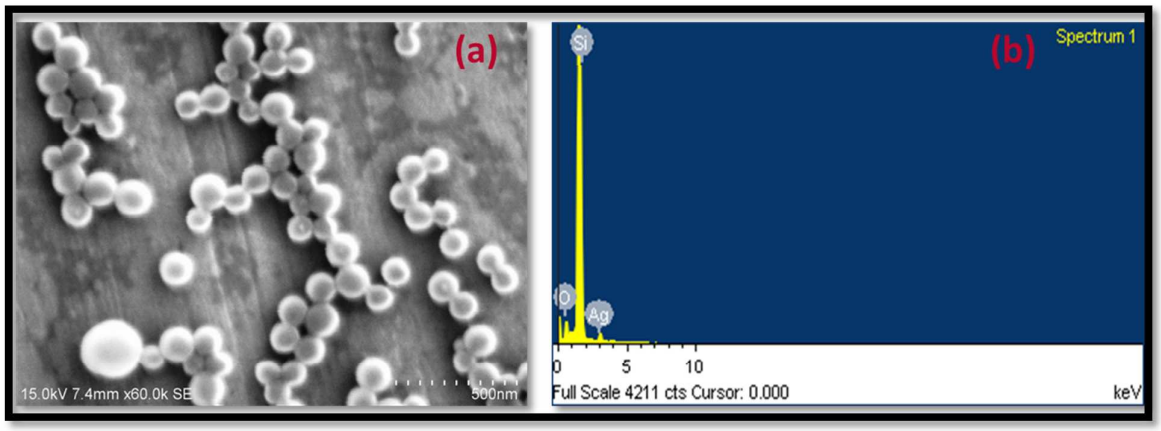
(a)
15.0kV 7.4mm x60.0k SE
500nm
(b)
Spectrum 1
Si
O
Ag
0
5
10
Full Scale 4211 cts Cursor: 0.000
keV

Figure 5

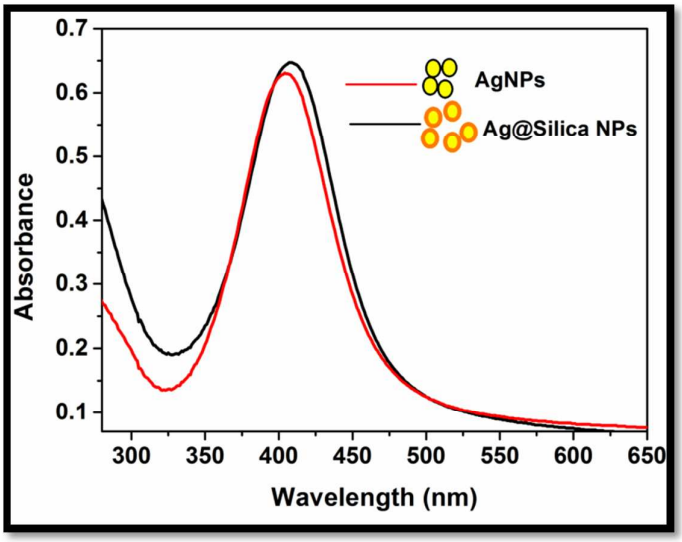
0.7
0.6
0.5
0.4
0.3
0.2
0.1
Absorbance
300
350
400
450
500
550
600
650
Wavelength (nm)
AgNPs
Ag@Silica NPs

Figure 6

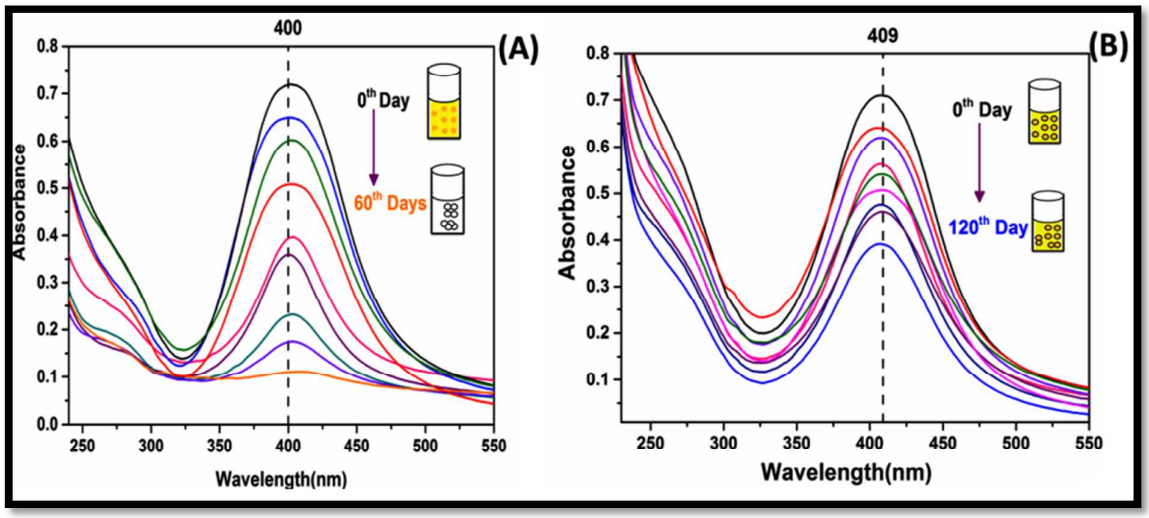
400
(A)
0th Day
60th Days
Absorbance
Wavelength(nm)
409
(B)
0th Day
120th Day
Absorbance
Wavelength(nm)

Figure 7

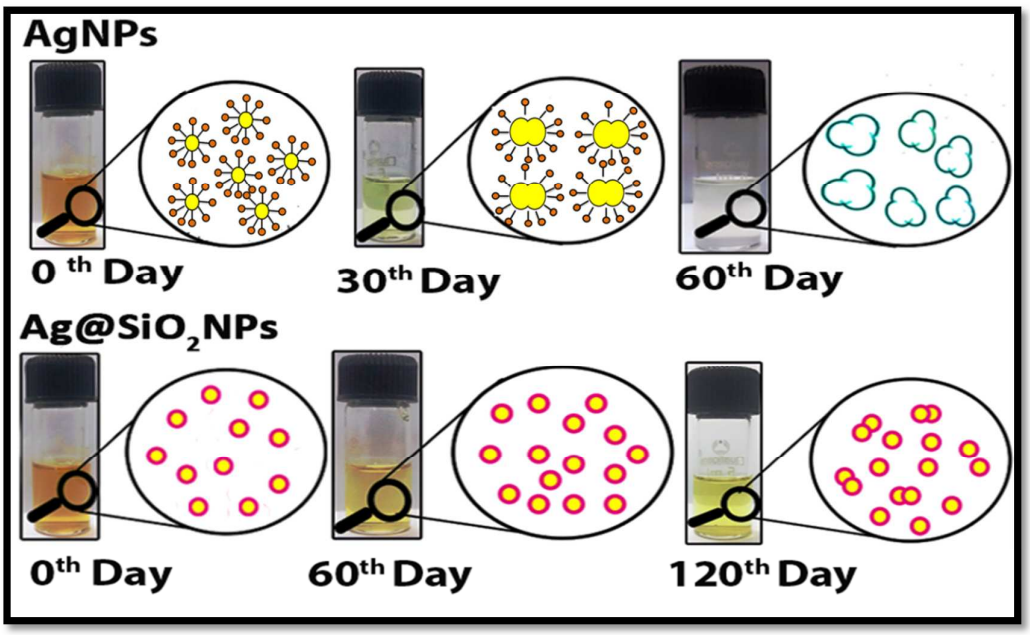
AgNPs
0 th Day
30th Day
60th Day
Ag@SiO2NPs
0th Day
60th Day
120th Day

Figure 8

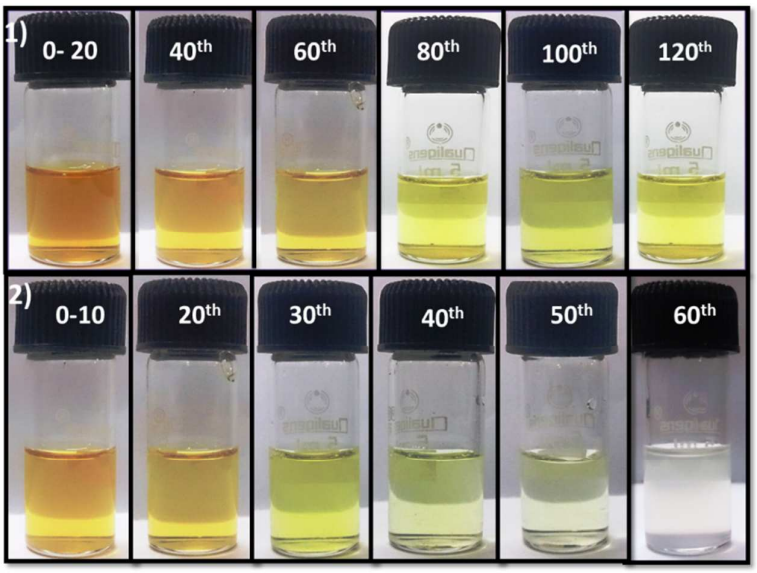
1)
0- 20
40th
60th
80th
100th
120th
2)
0-10
20th
30th
40th
50th
60th

Figure 9

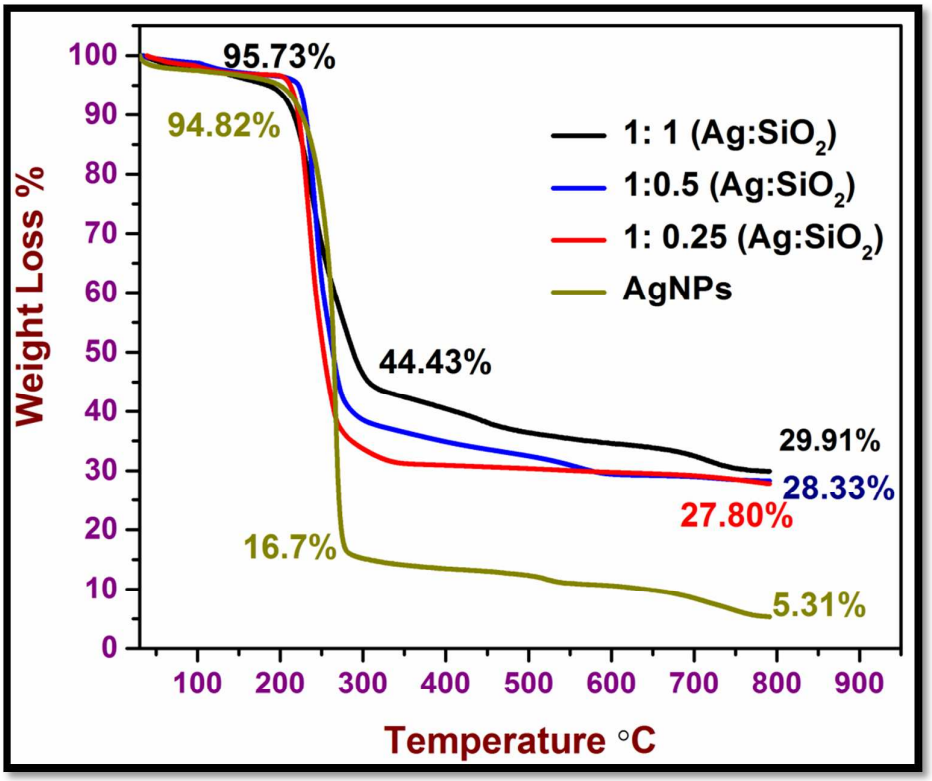
Weight Loss %
Temperature °C
95.73%
94.82%
44.43%
29.91%
28.33%
27.80%
16.7%
5.31%
1: 1 (Ag:SiO2)
1:0.5 (Ag:SiO2)
1: 0.25 (Ag:SiO2)
AgNPs

Figure 10

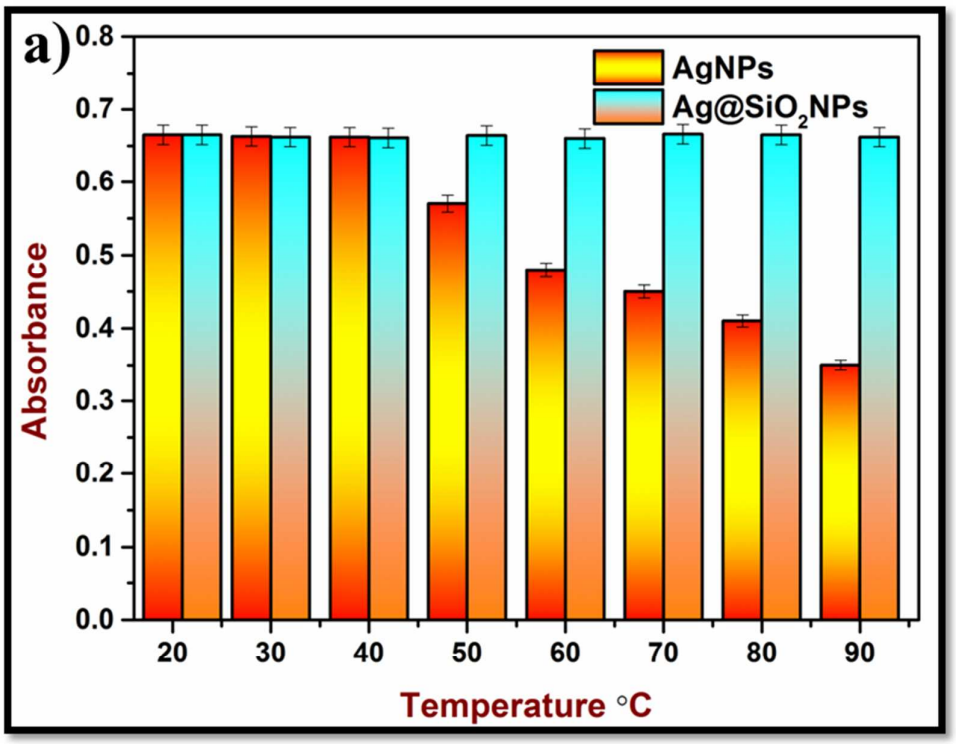
a)
AgNPs
Ag@SiO2NPs
Absorbance
0.0
0.1
0.2
0.3
0.4
0.5
0.6
0.7
0.8
20
30
40
50
60
70
80
90
Temperature °C

Figure 10

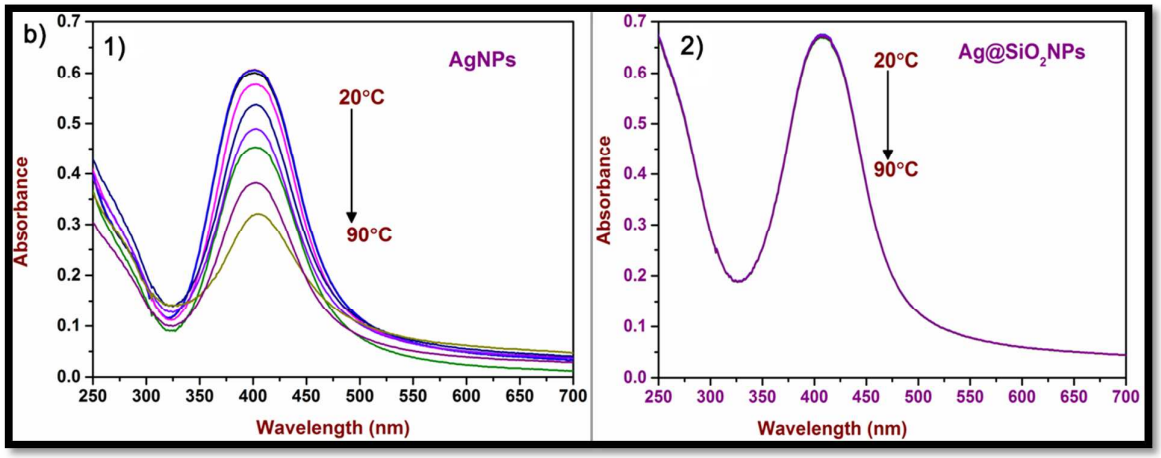
b)
1)
AgNPs
20°C
90°C
Absorbance
Wavelength (nm)
2)
Ag@SiO2NPs
20°C
90°C
Absorbance
Wavelength (nm)

Figure 11

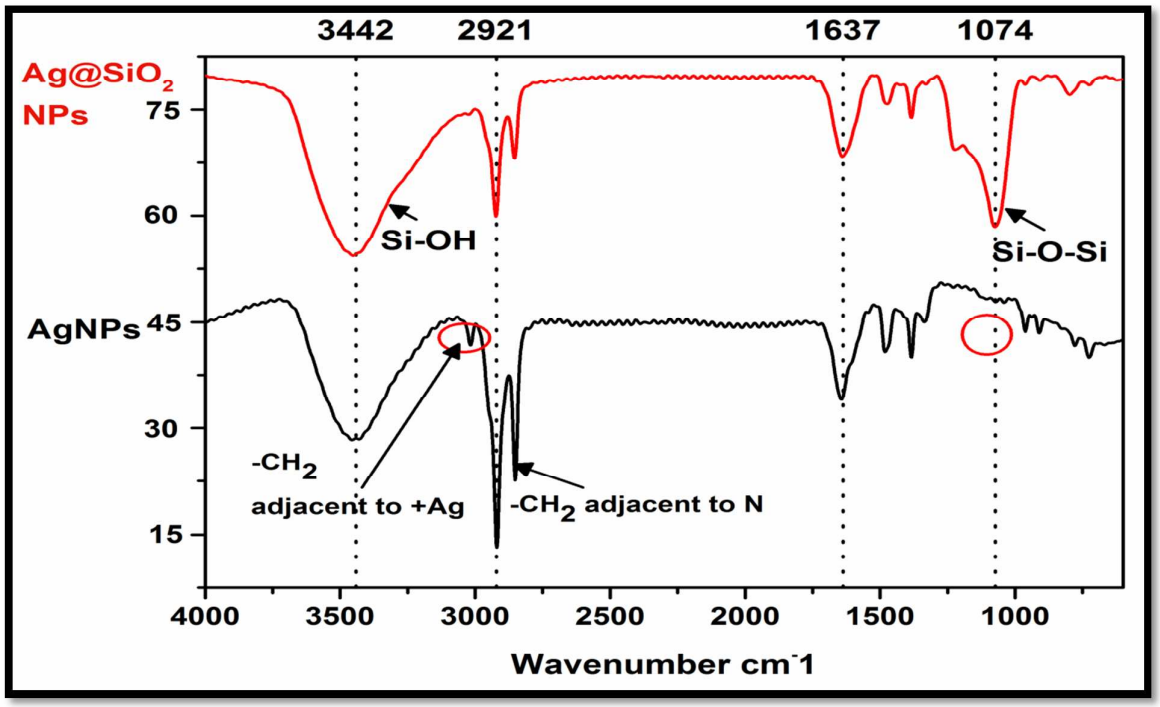
3442
2921
1637
1074
Ag@SiO2
NPs
AgNPs
75
60
45
30
15
Si-OH
Si-O-Si
-CH2
adjacent to +Ag
-CH2 adjacent to N
4000
3500
3000
2500
2000
1500
1000
Wavenumber cm-1

Figure 12

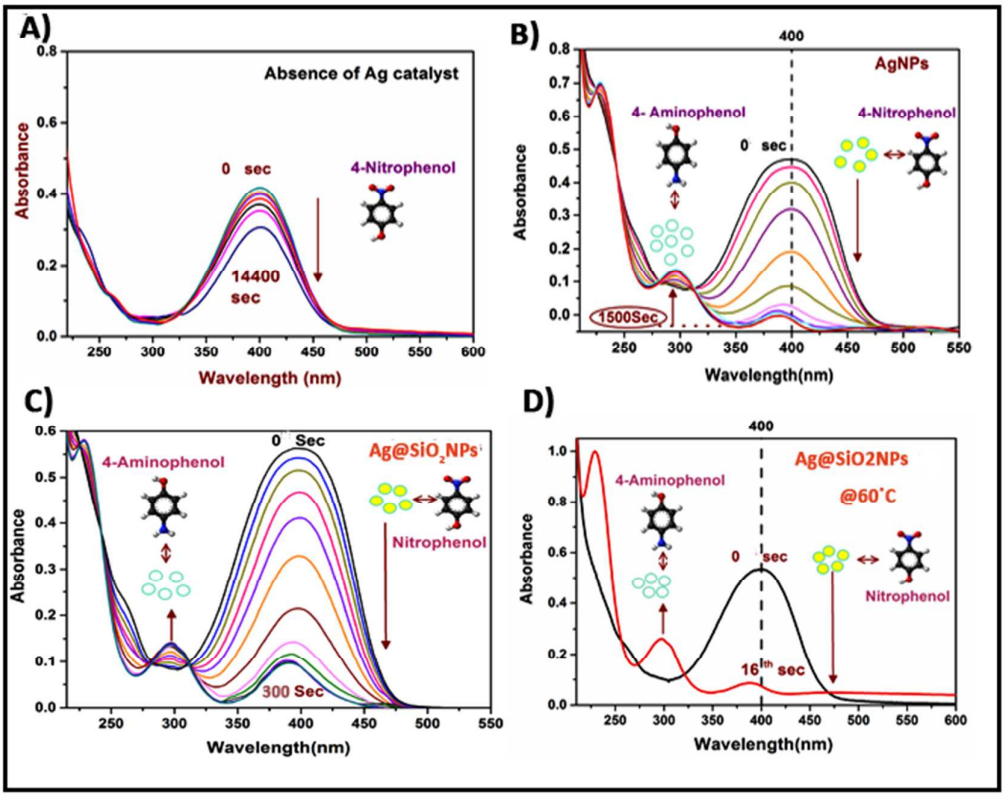
A)
Absence of Ag catalyst
0 sec
4-Nitrophenol
14400 sec
Absorbance
Wavelength (nm)
B)
AgNPs
4- Aminophenol
4-Nitrophenol
0 sec
1500Sec
Absorbance
Wavelength(nm)
C)
4-Aminophenol
0 Sec
Ag@SiO2NPs
Nitrophenol
300 Sec
Absorbance
Wavelength(nm)
D)
4-Aminophenol
Ag@SiO2NPs
@60°C
0 sec
Nitrophenol
16th sec
Absorbance
Wavelength(nm)

Figure 13

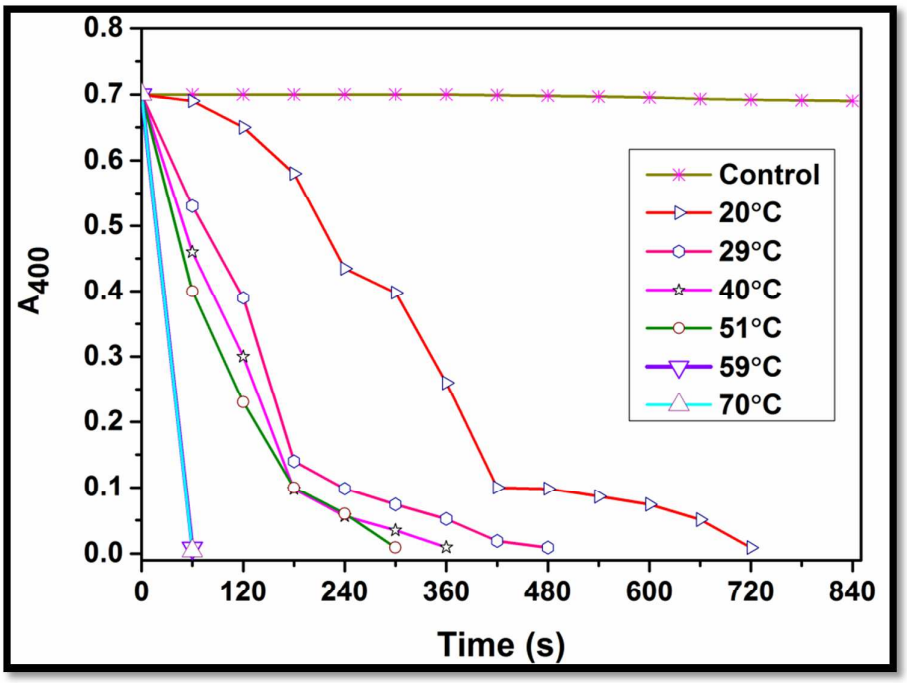
0.8
0.7
0.6
0.5
0.4
0.3
0.2
0.1
0.0
A400
0
120
240
360
480
600
720
840
Time (s)
Control
20°C
29°C
40°C
51°C
59°C
70°C

Figure 14

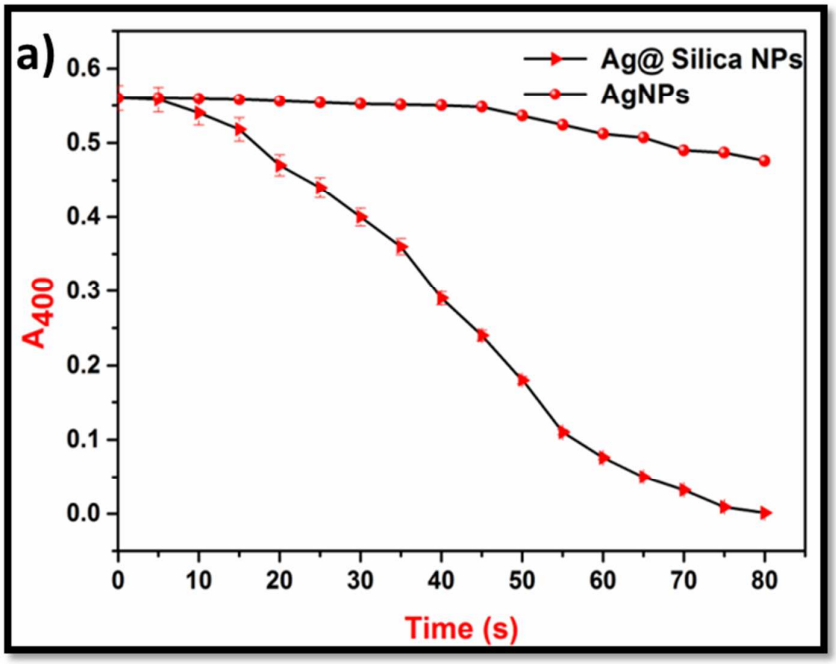
a)
Ag@ Silica NPs
AgNPs
A400
Time (s)
0.0
0.1
0.2
0.3
0.4
0.5
0.6
0
10
20
30
40
50
60
70
80

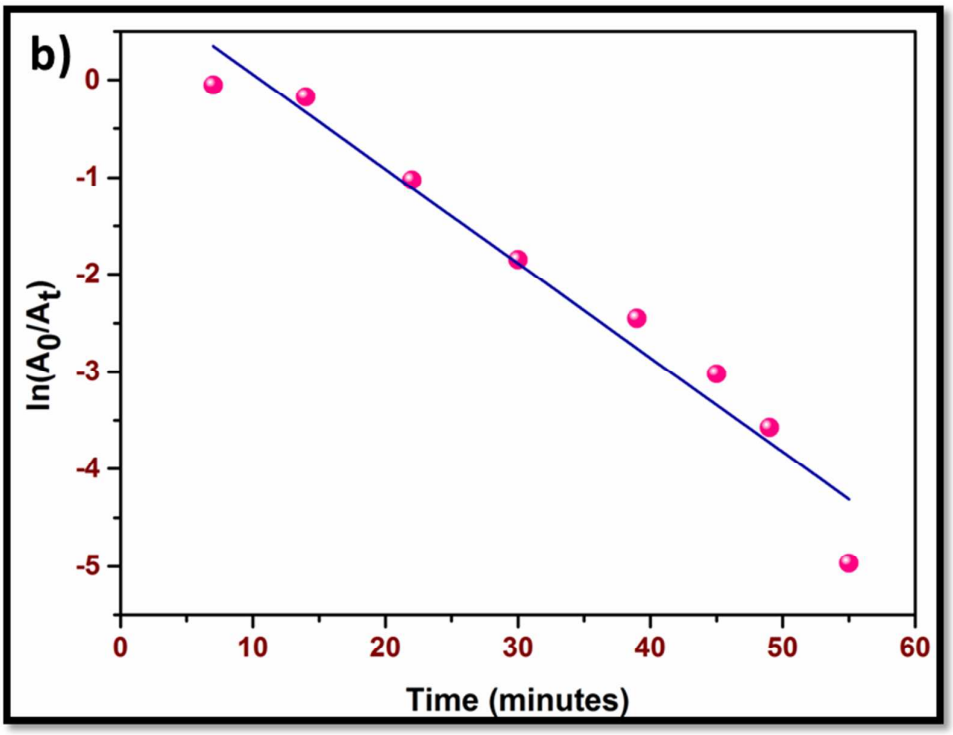
b)
0
-1
-2
-3
-4
-5
ln(A0/At)
0
10
20
30
40
50
60
Time (minutes)

Figure 15

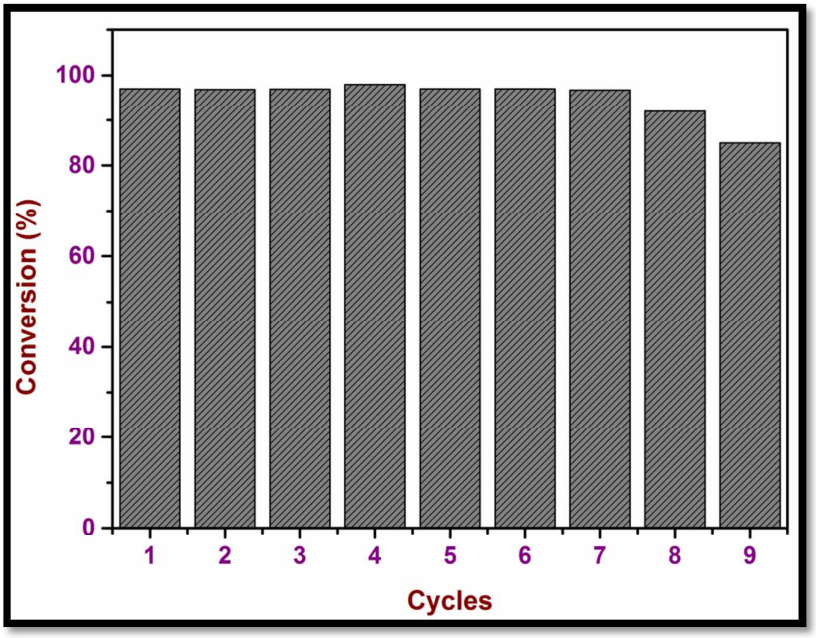

Table 1

S.no	Composite NPs formulation	$NaBH_4$ input (M)	Reaction time (sec) @ room temperature	Rate constant	Modifier /stabiliser
1	Ni core –Si shell	0.2	960	2.818×10^{-3} s^{-1}	EDTA [62]
2	NAP-Mg–Au(0)	0.01	150	7.6×10^{-3} s^{-1}	[63]
3	$Ag@SiO_2$	0.01	720	0.37 min^{-1}	PMAPTACb-PDMAEMA [25]
4	Ni NPs	0.2	Above 600	2.7×10^{-3} s^{-1}	CTAB, PEG-10000, gelatin [64]
5	Au(0)@TpPa-1	-	780	5.35×10^{-3} s^{-1}	TpPa-1 [65]
6	Dendrimer-Silver Nanocomposites	0.03	-	5.9×10^{-4} s^{-1}	poly(amido)amine dendrimers [26]
7	Fe3O4@SN/HPW@CG–Ag	0.2	420	0.53 min^{-1}	chitosan[66]
8	Nickel NPs	0.01	-	1×10^{-3} s^{-1}	spherical poly (acrylic acid) (PAA) brushes[67]
9	Au-Fe_3O_4	0.1	600	0.72 min^{-1}	oleate[68]
10	Fe_3O_4@PBLG@Au NPs	-	1620	-	poly(γ-benzyl-L-glutamate)[69]
11	G4-NH_2(Pd_x) DENs	0.2	-	5.82×10^{-3} s^{-1}	poly(amido)amine (PAMAM) dendrimer[70]
12	Ni/graphene NPs	0.132	Above 300	11.7×10^{-3} s^{-1}	-[22]
13	PPI dendrimer-palladium	0.03	720	-	PPI dendrimer[26]
15	AgNP-PA-3K	0.012	660	5.50×10^{-3} s^{-1}	polyamino oxanorbornenes[27]
16	Ag@Nanosilica		2400	5.35×10^{-3} s^{-1}	Rhizopus oryzae[71]
17	Au/Ag	0.015	150	-	DPS[24]
18	AuNP−CNT	0.1	-	62 μms^{-1}	CNT[72]
19	Au@ ESm	-	420	6.3×10^{-3} s^{-1}	ESm[73]
20	CD -AgNPs	0.007	1260	1.94×10^{-3} s^{-1}	Cyclodextrin[74]

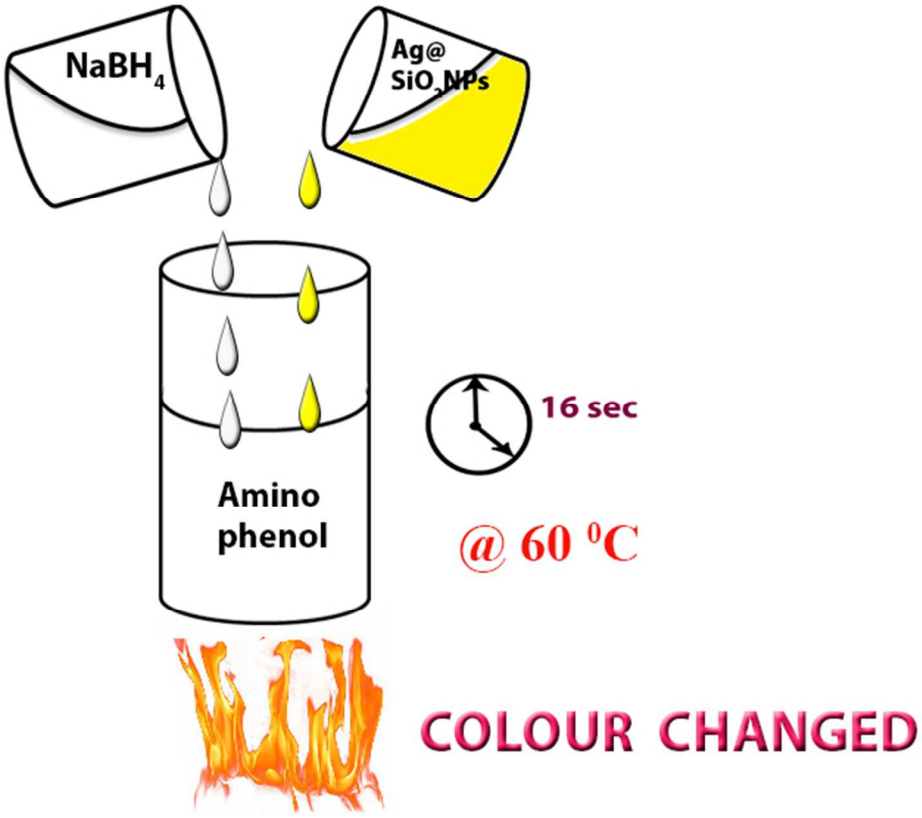

239x197mm (72 x 72 DPI)